JOURNAL OF MATERIALS SCIENCE **39** (2004) 141 – 149

Mechanism of *in situ* formation of AlN in Al melt using nitrogen gas

QINGJUN ZHENG, R. G. REDDY
Department of Metallurgical and Materials Engineering, The University of Alabama, Tuscaloosa, AL 35487-0202, USA
E-mail: rreddy@coe.eng.ua.edu

In situ processing of AlN particle reinforced aluminum composites was investigated using a gas bubbling method with nitrogen gas as the gaseous precursor and pure aluminum as the starting matrix in the temperature range of 1173–1573 K. The products were characterized using XRD, SEM, and EDS techniques. Experimental results showed that it is feasible to synthesize AlN particle reinforced Al composites *in situ* using purified nitrogen gas. Significant AlN was synthesized by bubbling deoxidized N_2 through Al melt. The AlN particles synthesized *in situ* were small in size (<10 μm) and were enriched in the top part of the product formed in the crucible. Directly bubbling commercial purity nitrogen gas did not lead to formation of significant AlN due to the deleterious effect of the trace oxygen impurities in the bubbling gas. The deleterious effect of trace oxygen impurities on the mechanism of formation of AlN in the Al-N system was critically analyzed from both thermodynamic and kinetic points of view. Chemisorption of O_2 molecules at the gas bubble-Al melt interface is more favorable and much faster than that of N_2, thereby inhibiting chemisorption of N_2 molecules. Significant AlN can be formed only at the content of oxygen below a critical value in the N_2 bubbling gas.

1. Introduction

Discontinuously reinforced Al alloy composites (DRACs) received great attention during the last decade due to their superior properties over the traditional metallic materials including tensile strength, stiffness, and wear resistance [1]. Moreover, their cost is lower than those of continuous reinforced Al alloy composites. Applications of DRACs have been increasing in many fields including defense, aerospace, automotive, electronic packing, sports and recreation.

Conventionally, DRACs are processed by incorporating the reinforcing particles into the matrix alloys through solidification techniques such as preformed infiltration and solid-state techniques such as powder metallurgy [2–7]. However, the optimum mechanical properties may not be achieved since the following reasons. First of all, the surface of the ceramic particles may be contaminated during their manufacturing. The surface contamination of ceramic particles may increase interfacial energy of the reinforcement-matrix interface, thereby weakening the interfacial bonding. Secondly, the ceramic particles may not be thermodynamically stable in the alloy matrix. During the process of manufacturing, secondary processing, and long-term service, especially at high temperatures, reactions may take place at the reinforcement-matrix interface and form unfavorable products. This weakens the interfacial bonding further. Therefore, the DRACs processed through conventional methods are far from optimal.

Another drawback of the DRACs through conventional techniques is their high production cost. The mechanical properties of DRACs are dependent on composition of the matrix alloy and size, dispersion and volume fraction of the reinforcing particles. Superior mechanical properties of DRACs require utilization of the small reinforcing particles, which are currently very expensive. Also, surface treatment of the reinforcing particles may be required to eliminate their surface contamination and to increase their thermodynamic stability in the conventional processing. This further increases production cost of the DRACs.

In situ processing of DRACs is promising since the equilibrium reinforcing particles are directly formed from the *in situ* chemical reaction. Since the reinforcing particles are formed directly from the low-cost materials, production cost of the DRACs can be lowered. Also, since the reinforcing particles are formed *in situ*, they are thermodynamically stable and free of surface contamination, yielding better interfacial properties. Additionally, by controlling the processing variables, the size of reinforcing particles may be optimized to give better mechanical properties. Owing to these potential advantages, the *in situ* methods have received increasing attention of materials scientists since 1990s. The recent research results on the synthesis and properties of *in situ* DRACs were reviewed by Tjong and Ma [8].

In situ processing of DRACs can be realized by many different approaches such as solid-solid reaction

process [9], solid-liquid reaction process [10, 11], direct metal oxidization process [12–14] and gas-bubbling method [15–18]. Among these *in situ* routes, the gas bubbling method, in which the reinforcing particles are formed from the reaction between molten metal and bubbling gas, has a great advantage. Since the availability of large contact area between the gaseous and liquidus reactants, a high rate of reinforcement formation may be achieved. Using the gas bubbling method, processing of TiC-Al and SiC-Al composites has been reported [15–18]. However, formation of AlN-Al composites has not been successful by means of this method for a long time. It was thought that formation of AlN by bubbling N-bearing gas (e.g., N_2 and NH_3) was not feasible due to the limitation of intrinsic kinetics such as passivation at the interface [19]. However, in our preliminary work [20–24], the equilibrium AlN-Al alloy composites were formed using this technique. In the present paper, feasibility and mechanism of the *in situ* formation of AlN and the effect of the trace oxygen impurities on the formation of AlN are discussed.

2. Experimental

The schematic diagram of the experimental setup is shown in Fig. 1. Experiments were carried out in the Lindberg vertical resistance tube furnace with a working temperature range of 773–1773 K. The furnace tube, made of stainless steel, was closed at the bottom end and sealable at the top end. The furnace cover, used for sealing the top end of the furnace tube, was water-cooled during the experiments. The alumina crucible of 100 ml, functioning as the reactor, was located in the uniform temperature region of the furnace tube. The gas bubbling tube is an alumina tube with a nozzle of diameter of 1.5 mm, which was merged into the melt near the bottom of the reactor in the bubbling process. In the experiments, the N_2 gas was passed through the gas cylinder, moisture trap, oxygen-removal furnace and flow meter and was then bubbled into the matrix melt through the gas bubbling tube. The moisture trap was used for the removal of trace moisture in the bubbling gas. The active material for the moisture-trapping is molecular sieve 13X, which could lower the moisture level below 10 ppb. The oxygen-removal furnace is filled with the copper turnings for removing the trace O_2 in the N_2 gas precursor. The oxygen-removal furnace was operated at 773 K. After deoxidation, the oxygen in nitrogen gas could be lowered to $\sim 10^{-6}$ Pa based on the thermodynamic estimation.

The temperature for formation of AlN was controlled by a Lindberg GS temperature controller with a type-S thermocouple (Thermocouple 1) positioned in the middle constant temperature region of the furnace. Thermocouple 2 with an end positioned at the wall of the reactor and with another end connected with a DP460 temperature monitor was used for measuring temperature in the reactor.

Pure Al of 99.9%, purchased from Aldrich, was used as the starting matrix material. Nitrogen gas of 99.998% from Airgas, was used as the bubbling gas. Argon gas of 99.999%, also from Airgas, was used for purging the furnace tube and for keeping an inert atmosphere.

The total weight of the starting matrix material, Al, was about 80 g for each experiment. The furnace tube was sealed with the furnace cover after setting the reactor, gas-bubbling tube, gas-purging tube, and thermocouples. Before heating, the reactor was vacuumed and then flushed by argon gas for three times. Throughout the subsequent process from furnace-heating to furnace-cooling, the flow rate of the argon gas was kept at $0.1\ \mathrm{L \cdot min^{-1}}$ so that the reactor was kept under an inert atmosphere. An opening in the furnace cover served as the exit for gas. After the Al melt reached the preset temperature (experimental temperature range: 1173–1573 K), N_2 gas bubbling was started. Following the gas bubbling, the electricity was turned off, allowing the products cool to room temperature in the furnace under argon atmosphere. The reaction process was monitored through an eyehole on the furnace cover.

The product was characterized by X-ray diffraction (XRD) for the phases, by scanning electron microscopy (SEM) for morphology, and by energy dispersive X-ray microanalyses (EDS) for micro-composition.

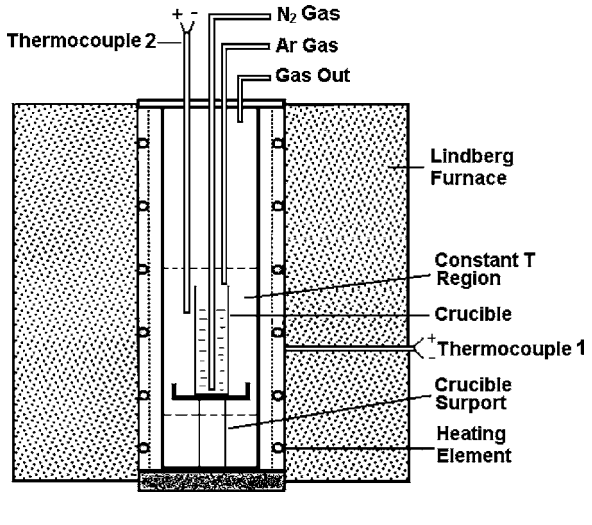

Figure 1 Schematic diagram of experimental setup.

3. Results

The experimental conditions and results are summarized in Table I, where the rate of AlN formation, R_{AlN}, was calculated based on the materials balance. Efforts were first made to form AlN by directly bubbling commercial N_2 (99.998% pure) through pure Al melt. As shown in Table I, however, gas-bubbling caused a slight weight loss of the matrix Al, suggesting that significant AlN was not formed. The product was characterized by XRD and is shown in Fig. 2, indicating the formation of little AlN. The slight weight loss of the matrix was due to evaporation of the molten Al during the gas-bubbling process.

Efforts were further made by bubbling deoxidized N_2 gas through Al melt at 1473 K. The partial pressure of O_2 in the N_2 bubbling gas was lowered to $\sim 10^{-6}$ Pa after deoxidation. It was found that significant AlN was formed. As shown in Table I, there was a weight gain

TABLE I Experimental conditions and results (starting matrix: 80 g; gas flow rate: 0.11 $L \cdot min^{-1}$; ΔW: weight change of the matrix after experiments; W_{AlN}: weight of AlN formed; R_{AlN}: rate of formation of AlN in $g \cdot min^{-1}$)

Exp. no.	Starting matrix	Gaseous precursor	T (K)	t (min)	ΔW (g)	W_{AlN} (g)	R_{AlN} ($g \cdot min^{-1}$)
1	Pure Al	Commercial N_2	1173	360	−0.21	–	–
2	Pure Al	Commercial N_2	1373	360	−0.35	–	–
3	Pure Al	Commercial N_2	1473	360	−0.49	–	–
4	Pure Al	Commercial N_2	1573	360	−0.61	–	–
5	Pure Al	Deoxidized N_2	1473	360	+2.52	7.38	0.0205
6	Pure Al	Deoxidized N_2	1473	320	+2.13	6.24	0.0195

"−": weight decrease after experiments; "+": weight increase after experiments.

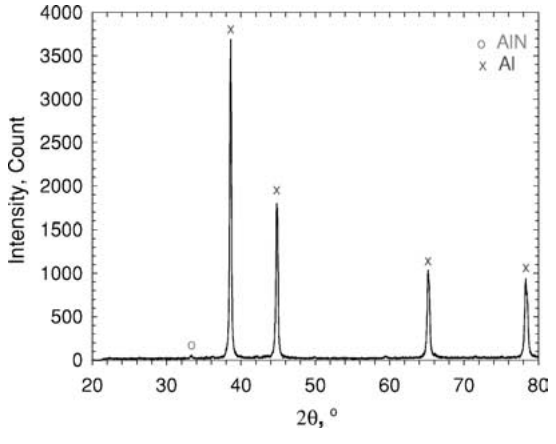

Figure 2 XRD pattern of the product formed by bubbling commercial N_2 gas through Al melt.

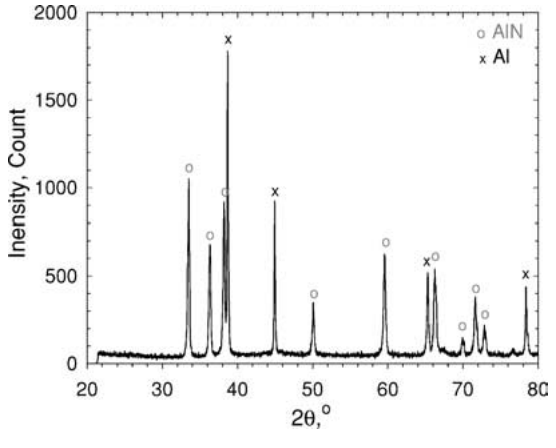

Figure 3 XRD pattern of top part of the product formed by bubbling deoxidized N_2 gas through Al melt.

of 2.52 g in the matrix alloy after bubbling for 360 min. Fig. 3 shows the XRD pattern of top part of the product formed *in situ* in the crucible. Strong AlN peaks were detected as well as those of Al in the top product, suggesting that the weight gain was due to the *in situ* formation of AlN. XRD analysis also showed that distribution of the AlN formed *in situ* is not uniform. As shown in Fig. 4, XRD peaks of AlN are very weak in the bottom product, indicating that the bottom product is pure aluminum. Further XRD characterization showed that the AlN formed *in situ* is enriched in the top part of the product and near the crucible wall.

Enrichment of AlN in the top part of the product and near the crucible wall was also proved by SEM and EDS analyses. Fig. 5 shows a typical SEM secondary

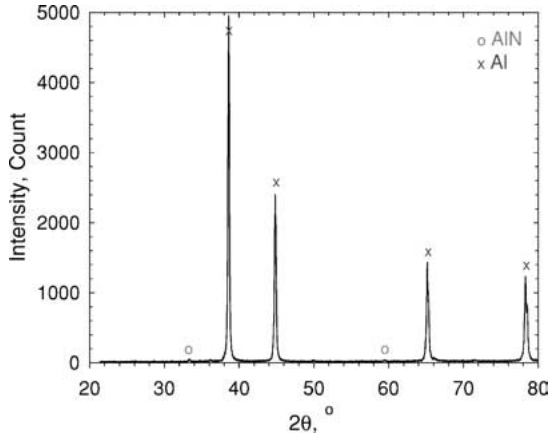

Figure 4 XRD pattern of bottom part of the product formed by bubbling deoxidized N_2 gas through Al melt.

electron image of top part of the product formed in the crucible. The EDS patterns corresponding to the regions with different colors in Fig. 5 are shown in Fig. 6. As suggested by Fig. 6a, the main compositions of the bright particulate domains in Fig. 5 are nitrogen and Al. Further EDS semi-quantitative analysis showed that the content of nitrogen and aluminum were about 48.2 and 51.8 at.% respectively. Therefore, the bright particulate domains in Fig. 5 are AlN particles. As suggested by Fig. 6b, the dark-color region in Fig. 5 is pure Al. The difference in colors of AlN particles and the matrix Al in Fig. 5 is due to the difference in their topographies. AlN particles have higher hardness and abrasive resistance than the matrix Al. Thus, the matrix Al was ground and polished faster than AlN in the process of sample preparation. Fig. 5 also shows that the AlN particles formed are small in size (<10 μm).

Fig. 7 is a typical SEM secondary electron image showing the morphology of the boundary region of the top AlN-Al composite and the bottom Al in the product formed in the crucible. As seen in the figure, there is a distinct boundary between the top AlN-Al composite and the bottom Al. In the side of Al, few AlN particles were detected while across the boundary AlN particles are enriched.

The above results showed that formation of AlN is feasible by reacting molten Al with the deoxidized N_2 bubbling gas. AlN particles formed *in situ* were found to be enriched in the top part of Al melt and near the crucible wall. The enrichment of AlN in the top part and near the crucible wall may be due to the difference in the surface energy among the phases including

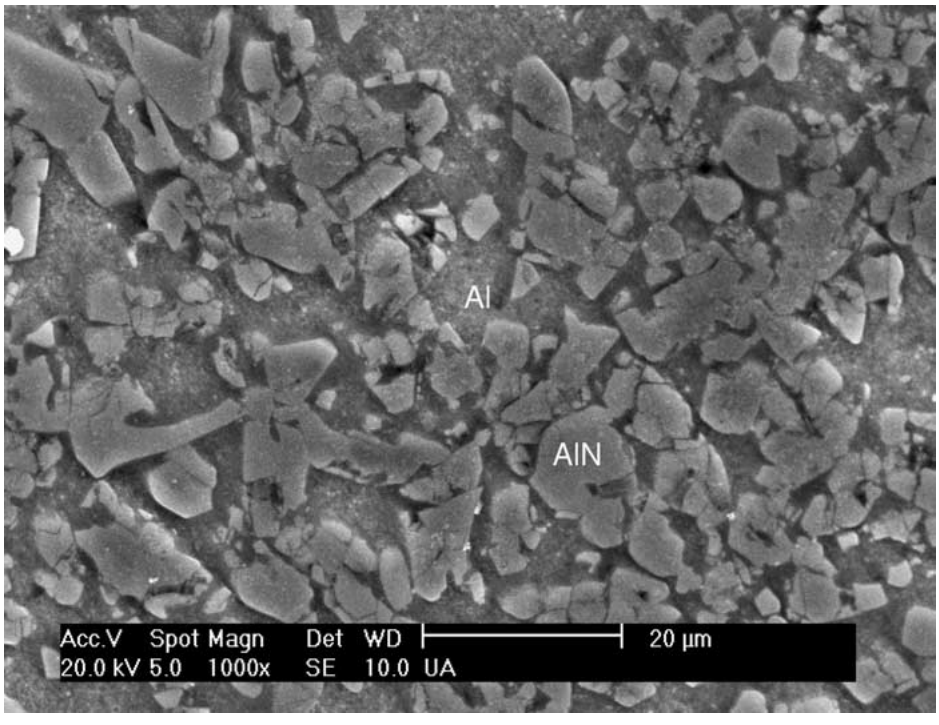

Figure 5 SEM secondary electron image of top part of the product formed by bubbling deoxidized N_2 gas through Al melt.

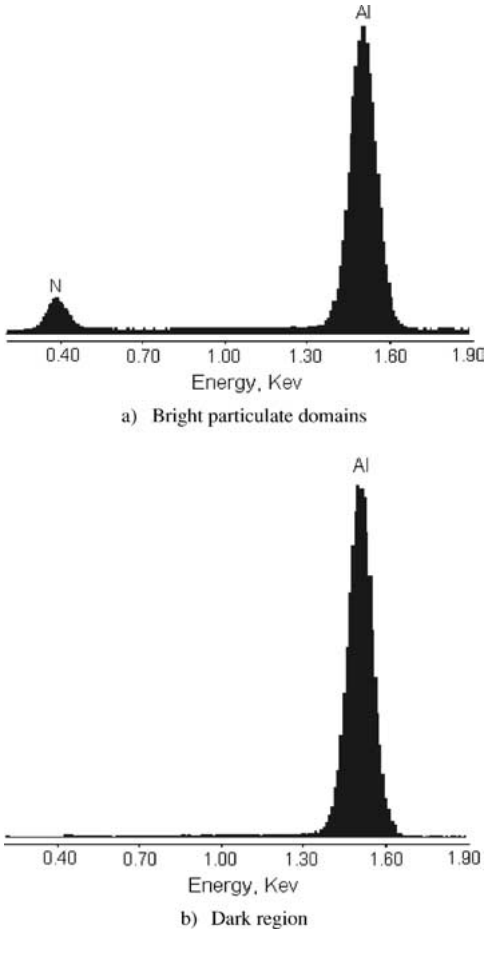

Figure 6 EDS patterns corresponding to (a) bright particulate domains and (b) dark region in Fig. 5.

the melt, gas, AlN particles formed *in situ*, and the crucible material. This phenomenon seems to be disadvantageous to the processing of *in situ* composites since it may cause the non-uniform dispersal of reinforcing particles in the matrix melt. However, an advantage can be taken by this phenomenon in the manufacturing of DRACs. Reddy and Wu [17] patented the use of the phenomenon for continuous processing of *in situ* DRACs. Akin to the froth flotation used in mineral processing, the ceramic particles formed *in situ* can be enriched in "metal foams" on the top of melt by controlling the process and materials parameters. The "metal foams" containing the reinforcing particles can then be bubbled out of the reactor and collected in the composite collector to form the composite. During the process of composite formation, the Al alloy can be added in the reactor at regular intervals. The DRACs can thus be processed continuously.

4. Discussions

When N_2 is bubbled into Al melt, solid AlN may be formed from the heterogeneous reaction between molten Al and N_2 gas given by:

$$\mathrm{Al(l)} + 1/2\mathrm{N_2(g)} = \mathrm{AlN(s)} \tag{1}$$

Since the activity of Al is unity for pure Al melt, Gibbs energy change of the reaction, $\Delta G_{(1)}$, is:

$$\Delta G_{(1)} = \Delta G^{\mathrm{o}}_{(1)} - \frac{1}{2} RT \ln P_{\mathrm{N_2}} \tag{2}$$

where $\Delta G^{\mathrm{o}}_{(1)}$ is the Gibbs energy change of the reaction given by Equation 1 at standard condition, and $P_{\mathrm{N_2}}$ is the total pressure of N_2 in the gas bubble in atm, which is the sum of the atmospheric pressure, P_{o} (=1 atm), and the static pressure of the Al melt, $\rho_{\mathrm{L}} g h_{\mathrm{L}}$. Since the density, ρ_{L}, and the height of matrix melt, h_{L}, were small in the experiments, $\rho_{\mathrm{L}} g h_{\mathrm{L}}$ is negligible compared with P_{o}. Therefore, $\Delta G_{(1)}$ approximates to

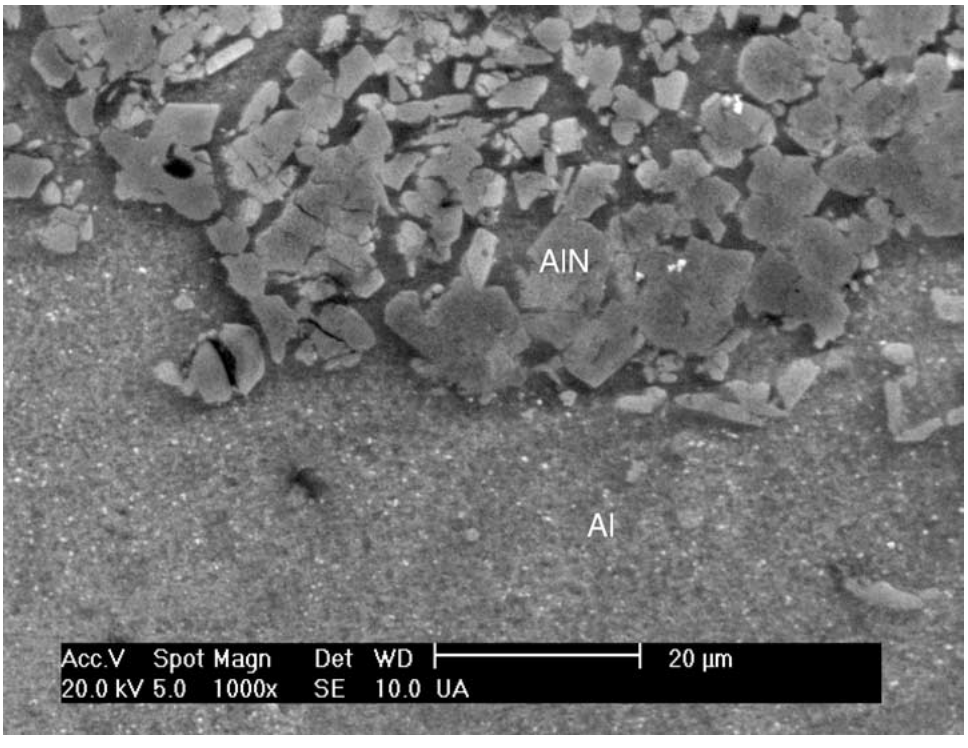

Figure 7 SEM secondary electron image of the boundary region between the top AlN-Al composite and bottom Al in the product formed by bubbling deoxidized N_2 gas.

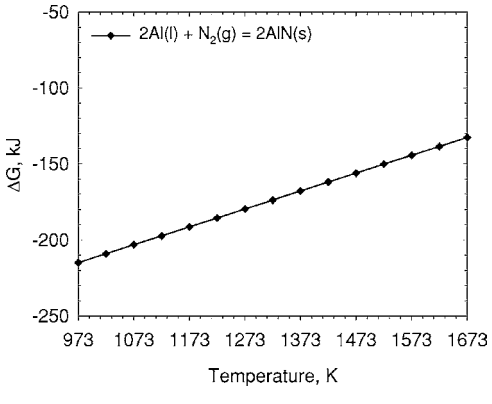

Figure 8 Gibbs energy change of the reaction: $Al(l) + 1/2N_2(g) = AlN(s)$.

$\Delta G^{o}_{(1)}$, which was calculated using the Chemical Reaction Equilibrium Software, HSC, and is plotted in Fig. 8 as the function of temperature. $\Delta G_{(1)}$ is negative, showing that formation of AlN is thermodynamically favorable in the temperature range of 973–1673 K. However, significant AlN was not formed when the N_2 gas of commercial grade was directly bubbled. Significant AlN was formed only by bubbling the deoxidized N_2 gas. This shows that trace oxygen impurities (mainly O_2 and H_2O) in the bubbling gas have a strong deleterious effect on the nitridation of Al. The deleterious effect of trace oxygen impurities on nitridation of molten Al was also observed by Scholz *et al.* [12] and Swaminathan *et al.* [25]. Scholz *et al.* [12] investigated the formation of AlN-Al composites by direct nitridation of Al-Mg-Si melt. In the experiments, nitrogen was introduced above the alloy melt. It was found that significant AlN could not be formed under flowing commercial N_2 atmosphere but was formed under flowing deoxidized N_2 atmosphere. Swaminathan *et al.* [25] studied the influence of oxygen impurities on formation of the AlN-Al composites by infiltration method. They found that increasing oxygen content from 10 ppm upwards decreased the nitride content in the matrix from 64 to 6 vol%. All these evidenced the deleterious effect of trace oxygen on nitridation of aluminum. Trace oxygen was also found to be deleterious to nitridation of other metals such as gallium and indium [26]. To understand mechanism of the deleterious effect of trace oxygen impurities, thermodynamics and kinetics of nitridation of molten Al are analyzed.

4.1. Thermodynamic analysis

When the commercial N_2 gas is bubbled, apart from the reaction shown in Equation 1, the oxygen impurities may react with molten Al through the reactions given by:

$$4Al(l) + 3O_2(g) = 2Al_2O_3(s) \quad (3)$$

$$2Al(l) + 3H_2O(g) = Al_2O_3(s) + 3H_2(g) \quad (4)$$

Both reactions are competitive with that given by Equation 1. The preference of AlN formation is dependent on gaseous composition and temperature and can be evaluated based on the reactions:

$$4AlN(s) + 3O_2(g) = 2Al_2O_3(s) + 2N_2(g) \quad (5)$$

$$2AlN(s) + 3H_2O(g) = Al_2O_3(s) + N_2(g) + 3H_2(g) \quad (6)$$

If Gibbs energy changes of the above two reactions are positive, the reactions proceed toward the left and AlN has the preference to form. Hence, the conditions for formation of AlN are given by:

$$P_{O_2} \leq P_{N_2}^{\frac{2}{3}} \cdot \exp\left(\frac{\Delta G^{o}_{(5)}}{3RT}\right) \tag{7}$$

$$\frac{P_{H_2O}}{P_{H_2}} \leq P_{N_2}^{\frac{1}{3}} \exp\left(\frac{\Delta G^{o}_{(6)}}{3RT}\right) \tag{8}$$

Considering that H_2O, H_2, and O_2 are balanced by the reaction:

$$2H_2O(g) = 2H_2(g) + O_2(g) \tag{9}$$

Equations 7 and 8 are equivalent. The standard Gibbs energy change of the reaction shown in Equation 7, $\Delta G^{o}_{(5)}$, is given based on HSC by:

$$\Delta G^{o}_{(5)} = -2063600 + 190.4T \ \ J \tag{10}$$

Since the pressure of N_2, P_{N_2}, approximates to 1 atm when N_2 is bubbled, the permissible partial pressure of O_2, P_{O_2}, in the N_2 gas for formation of AlN can thus be calculated based on Equations 7 and 10. The calculated results are shown in Fig. 9. As shown, the permissible partial pressure of O_2 is extremely low. It is $\sim 10^{-17}$ Pa at 1473 K. To form AlN, the actual partial pressure of O_2, which is contributed by both O_2 and moisture in the N_2 precursor, is required to be below the permissible value at the reaction sites. A similar thermodynamic analysis was made by Scholz and Greil [12]. They pointed out that nitridation of the Al-Si-Mg melt required extremely low O_2 partial pressure of $\sim 10^{-15}$ Pa at 1473 K.

The above thermodynamic analysis explains well why significant AlN was not formed when commercial N_2 gas was used. In the commercial N_2 gas, the content of oxygen impurities was ~100 ppm, i.e., its partial pressure was ~10 Pa in the N_2 gas bubble. Since this value is much higher than the thermodynamic permissible limit for the nitridation reaction, AlN can not be formed. During the rising process of gas bubble in the matrix melt, the content of oxygen impurities in the N_2 gas may be lowered owing to the heterogeneous reactions shown in Equations 3 and 4. However, since the residence time of a gas bubble in the matrix melt is short, the partial pressure of O_2 may not be lowered below the permissible limit during the rising process. A long incubation period for lowering the content of oxygen below a threshold value for significant nitridation reaction was proved by direct nitridation of Al-Mg-Si melt [12]. Therefore, the partial pressure of O_2 in the N_2 gas bubble may always be beyond the permissible limit during the residence of the gas bubble in the melt. As the result, significant AlN can not be formed.

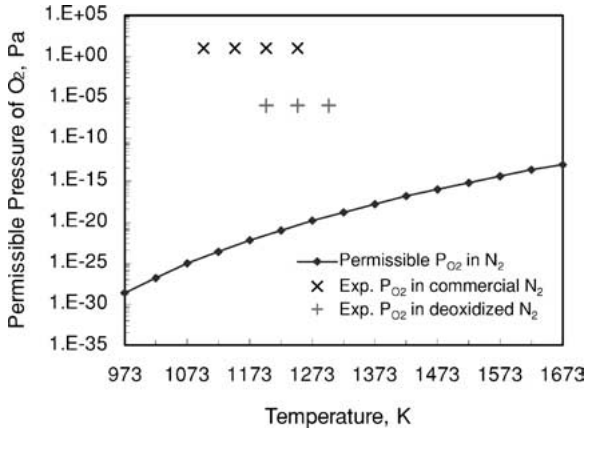

Figure 9 Permissible partial pressure of O_2 in the N_2 bubbling gas for formation of AlN.

The above thermodynamic analysis, however, can not give satisfactory interpretation on the formation of significant AlN by bubbling deoxidized N_2 gas. After deoxidization, the partial pressure of oxygen impurities could be lowered to $\sim 10^{-6}$ Pa in the bubbling gas. As shown in Fig. 9, this value is much lower than that before deoxidation but still beyond the thermodynamically permissible limit. However, significant AlN was formed. Formation of AlN at the content of oxygen above the thermodynamic permissible value was also observed by Swaminathan *et al*. [25]. This suggests that the reactions shown in Equations 3–6 could not represent the whole mechanism of effect of the trace oxygen impurities. During the above thermodynamic analysis, equilibrium product, Al_2O_3, was assumed to be formed. However, during the oxidation process of Al melt, chemisorption of oxygen occurs at the surface of Al before equilibrium Al_2O_3 is precipitated. At very low content of oxygen, oxygen may not be available for precipitation of equilibrium Al_2O_3. Therefore, kinetic analysis of the heterogeneous reaction process of AlN formation is required to give a better picture of the mechanism of the deleterious effect of trace oxygen impurity.

4.2. Kinetic analysis

When N_2 gas is ejected into Al melt through the submerged nozzle, its flow feature in the melt is determined by the nozzle size, gas flow rate, and properties of Al melt including density, viscosity, and surface energy. Continuum flow (also called as ejected flow) is formed when the gas flow rate is high. At a small gas flow rate, diffusive bubble flow is formed, in which the gas bubbles are formed at nozzle separately and then float in the melt due to the buoyancy force. As the gas bubbles arrive at the melt surface, they break up and merge into atmosphere. AlN is formed during the rising process of gas bubbles from the heterogeneous reaction given by Equation 1. The reaction process for formation of AlN can be described by the two-film model (schematized in Fig. 10) [27]. As shown in Fig. 10, the whole process includes the following four steps:

Step 1: mass transfer of N_2 molecules through the gas boundary layer to the gas bubble-Al melt interface:

$$N_2\left(P_{N_2,o}\right) \xrightarrow{\text{diffusion}} N_2\left(P_{N_2,i}\right) \tag{11}$$

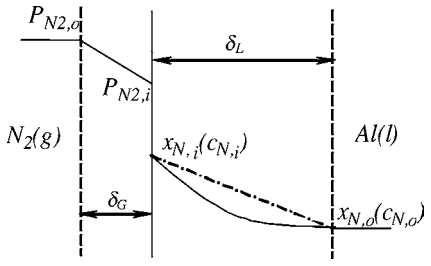

Figure 10 Two-film model describing the mechanism of the Al melt-N_2 gas reaction process.

Step 2: chemisorption of N_2 molecules at the interface:

$$\frac{1}{2}\mathrm{N_2(g)} \leftrightarrows \mathrm{N(chemisorbed)} \tag{12}$$

Step 3: mass transfer of nitrogen atoms in the liquid boundary layer:

$$\mathrm{N}(x_{\mathrm{N,i}}) \xrightarrow{\text{diffusion}} \mathrm{N}(x_{\mathrm{N,o}}) \tag{13}$$

Step 4: growth of solid AlN particles at the interface, in the liquid boundary layer, and in the bulk Al melt:

$$\mathrm{N(in\ liquid)} + \mathrm{Al(l)} = \mathrm{AlN(s)} \tag{14}$$

Among these steps, Step 1, the mass transfer of N_2 molecules in the gas boundary layer, which is driven by its partial pressure gradient, is faster than Step 3, the mass transfer of nitrogen atoms in the liquid boundary layer, which is driven by its concentration gradient. As shown in Equation 12, Step 2, the chemisorption of N_2 molecules at the interface involves adsorption of N_2 molecules at the interface and desorption of the chemisorbed nitrogen atoms. The total neat chemisorption rate of N_2, $r_{\mathrm{N,a}}$, is given by:

$$r_{\mathrm{N,a}} = \frac{1}{A_{\mathrm{B}}}\frac{\mathrm{d}n_{\mathrm{N}}}{\mathrm{d}t} = k_{\mathrm{a}}P_{\mathrm{N_2,i}}^{\frac{1}{2}} - k_{\mathrm{d}}x_{\mathrm{N,i}}$$
$$= k_{\mathrm{a}}\left(P_{\mathrm{N_2,i}}^{\frac{1}{2}} - \frac{x_{\mathrm{N,i}}}{K_{(12)}}\right) \tag{15}$$

where A_{B} is the surface area of the gas bubble; n_{N} is the moles of chemisorbed nitrogen atoms at the interface; t is the bubbling time; k_{a} and k_{d} are the chemisorption and desorption constants respectively; $P_{\mathrm{N,i}}$ and $x_{\mathrm{N,i}}$ are the pressure of N_2 gas and the concentration of chemisorbed nitrogen atoms at the interface respectively; and $K_{(12)}$ $(=\frac{k_{\mathrm{a}}}{k_{\mathrm{d}}})$ is equilibrium constant of the chemisorption reaction given by Equation 12. Based on collision theory and activated complex theory, k_{a} for the chemisorption of a gas at the clean uniform surface, is given by [28]:

$$k_{\mathrm{a}} = c(2\pi MRT)^{-\frac{1}{2}}\exp\left(-\frac{E_{\mathrm{a}}}{RT}\right) \tag{16}$$

where c is a constant, M is the molar mass of the gas molecule, R is the gas constant, T is temperature, and E_{a} is the activation energy for chemisorption of the gas at the interface. Thus the overall neat chemisorption rate of N_2, $r_{\mathrm{N,a}}$, can be reorganized as:

$$r_{\mathrm{N,a}} = c(2\pi MRT)^{-\frac{1}{2}}\left(P_{N_2,i}^{\frac{1}{2}} - \frac{x_{\mathrm{N,i}}}{K_{(12)}}\right)\exp\left(-\frac{E_{\mathrm{a}}}{RT}\right) \tag{17}$$

Equation 17 indicates that the rate of N_2 chemisorption at the interface is dependent on the partial pressure of N_2 and concentration of nitrogen atoms at the interface, the activation energy barrier, and temperature. Based on the quantum mechanical calculation [29], E_{a} for chemisorption of N_2 molecules at the surface of Al melt is very high (308 $\mathrm{kJ \cdot mol^{-1}}$). Therefore, Step 2 may be slow. The rate of this step is strongly affected by the impurities in the gas and the surface state. Step 4, the growth of AlN particles (as shown in Equation 14) involves nucleation and growth of AlN crystals from nitrogen and aluminum atoms. The rate of Step 4 is determined by the concentration of nitrogen atoms, activation energy barrier of nucleation and growth of AlN crystals, and the undercooling ($\Delta T = T_{\mathrm{m}} - T$). Since the melting point, T_{m}, of AlN is very high (≈3073 K), very high undercooling can be provided under the experimental condition of this research. So, Step 4 is also fast. Hence, Steps 2 and 3 are slow among the four steps. Since the impurities in N_2 bubbling gas affect the rate of Step 2 but not the rate of Step 3, the strong deleterious effect of oxygen impurities in the N_2 bubbling suggests that Step 2, the chemisorption of N_2 gas at the interface, is the rate-controlling step. Therefore, the deleterious effect of trace oxygen impurities on formation of the AlN is due to its deleterious effect on the chemisorption of N_2 molecules at the interface.

To understand better the deleterious effect of oxygen impurities on the chemisorption of N_2 molecules, the chemisorption of a diatomic homo-nuclei gas is first considered. Fig. 11 shows a simple model describing the adsorption of a diatomic gas at the metal surface [30]. It is assumed that the metal surface in contact with the gas phase is subjected to continuous collision by gas molecules. When a gaseous molecule approaches the surface within a few atomic distance of the surface, induced-dipole interaction known as Van der Waals force will be created. If enough of the perpendicular component of the molecule's momentum is dissipated into the surface during the interaction, the approaching molecule will be trapped in a weak-bonded state, i.e., physisorption. Otherwise, the gas molecule will be repelled into the gas, i.e., reflection. Normally, physisorption is accompanied by a small decrease in

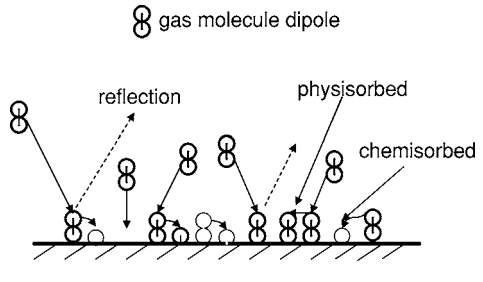

Figure 11 Schematic diagram of a gas surface adsorption model [30].

Gibbs energy of the system and does not have activation energy barrier. Thus it takes place at a very high rate independent of the gases. Dependent on the gained energy and the activation energy barrier, the physisorbed molecule may desorb or interact further with the surface to form stronger chemical bond, i.e., get chemisorbed after a while. Chemisorption is accompanied by significant reduction of Gibbs energy of the system and is characterized by strong chemical bonding between the gas atoms and those of metal at surface. The activation energy barrier is due to the reconstruction of chemical bond. For the gas with high affinity to the interface, the activation energy barrier is small. Therefore the transition from the physisorbed state to the chemisorbed state is fast or instantaneous. For the gas with low affinity to the interface, however, the physisorbed state can transmit into chemisorbed state only when it gains sufficient energy to overcome the high activation energy barrier; or it may desorb after a while. Hence, the chemisorption rate is low.

Fig. 12 shows the schematic diagram of Gibbs energy change for the adsorption of N_2-O_2 pair at the surface of Al melt. As shown in Fig. 12, there is not an obvious physisorbed state for adsorption of O_2. Since without obvious activation energy barrier, chemisorption of O_2 is instantaneous [29]. Also, chemisorption of O_2 is accompanied by a significant reduction in the Gibbs energy of the system. For chemisorption of N_2 gas, the intermediate Step, physisorption, is present. Since transition from the physisorbed state to the chemisorbed state requires overcoming a high activation energy barrier (308 kJ $\cdot$ mol^{-1}), not all of the physisorbed N_2 can get chemisorbed. Only those obtaining sufficient energies can be chemisorbed while most other physisorbed N_2 molecules are desorbed after staying at the surface for a while. Thus, the rate of chemisorption of N_2 is much slower than that of O_2. As shown in Fig. 12, chemisorption of a N_2 molecule can also lower Gibbs energy of the system, however, the decrease in the Gibbs energy is smaller than that caused by chemisorption of an O_2 molecule. Thus, chemisorption of O_2 molecules has the preference than that of N_2 molecules, that is, the chemisorbed nitrogen atoms can be desorbed by the O_2 molecules reaching the same sites. Desorption of chemisorbed nitrogen atoms by O_2 molecules at the surface of Al melt can be given by:

$$2\mathrm{N(chemisorbed)} + \mathrm{O_2(g)} = \mathrm{N_2(g)} + 2\mathrm{O(chemisorbed)} \quad (18)$$

Since O_2 has the preference to be chemisorbed and its chemisorption is much faster than that of N_2, chemisorption of N_2 is very sensitive to the oxygen impurities. N_2 can not be chemisorbed when the oxygen impurities are over a threshold limit in the N_2 atmosphere and significant AlN can not be formed. The threshold limit represents the real permissible partial pressure of O_2 in N_2 gas for formation of AlN, which should be calculated based on the reaction given by Equation 18, but not based on the reaction given by Equation 5. Unfortunately, in absence of thermodynamic data on the gaseous adsorption at the surface of metal melt, the permissible partial pressure of O_2 for formation of AlN can still not be calculated. Swaminathan *et al*. [25] suggested that it was below $\sim$0.01 Pa in N_2 gas of 1 atm. For the commercial N_2 gas, the partial pressure of O_2 was about $\sim$10 Pa, higher than the suggested permissible limit, so significant AlN was not formed. For the deoxidized N_2 gas, the partial pressure of O_2 was about $\sim 10^{-6}$ Pa, below the suggested value. Thus, chemisorption of N_2 was possible at the active sites, where O_2 was not available. Further, the nitrogen atoms chemisorbed at some active sites may have diffused into the melt before O_2 molecules can arrive at the same sites since its low availability. As the result, significant AlN was formed.

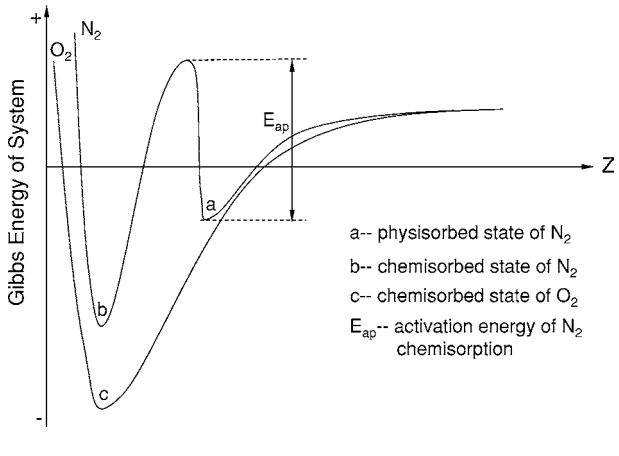

Figure 12 Diagram of energy change of the system caused by chemisorption of N_2-O_2 pair.

5. Summary

In situ processing of AlN particle reinforced Al composites was investigated using the gas bubbling method. Formation of AlN reinforcing particles by bubbling deoxidized N_2 gas through Al melt is technically feasible. The AlN particles formed *in situ* are small in size ($<10\,\mu$m) and are enriched in the top part of the product formed in the crucible.

Trace oxygen impurities have strong deleterious effect on formation of AlN. When commercial N_2 gas was bubbled, significant AlN was not formed although formation of the AlN is thermodynamically favorable. When deoxidized N_2 gas was bubbled, significant AlN was formed in the top part of the Al melt and near the crucible wall. The deleterious effect of oxygen impurities is due to its inhibition to the chemisorption of N_2 molecules at the interface. Chemisorption of O_2 at the interface can lower the Gibbs energy of the system greater than that of N_2 and so has the preference. Additionally, chemisorption of O_2 at the surface of Al melt does not have obvious activation energy barrier and is instantaneous. On the other hand, chemisorption of N_2 molecules requires overcoming a huge activation energy barrier and is very slow. Hence, significant AlN can be formed only when the O_2 content is below a critical value in the N_2 bubbling gas.

Acknowledgements

The authors are pleased to acknowledge the financial support for this research by National Science Foundation (DMI 9714321).

References

1. R. G. REDDY, *Comp. Manufac.* **14** (1998) 5.
2. P. A. EARVOLINO, M. E. FINE, J. R. WEERTMAN and V. R. PARAMESWARAN, *Scripta Metall.* **26** (1992) 945.
3. A. M. SAMUEL, H. LIU and F. H. SAMUEL, *J. Mater. Sci.* **28** (1993) 6785.
4. M. K. AGHAJANIAN, J. P. BIEL and R. G. SMITH, *J. Amer. Ceram. Soc.* **77** (1994) 1917.
5. J. U. EJIOFOR, G. F. FERNANDO and R. G. REDDY, *J. Mater. Sci.* **33** (1998) 4029.
6. J. L. ESTRADA, E. NICOLAS and E. J. LAVERNIA, *J. Mater. Syn. Proc.* **5** (1997) 77.
7. V. KEVORKIJAN, *Adv. Mater. Proc.* **155** (1999) 27.
8. S. C. TJONG and Z. Y. MA, *Mater. Sci. Eng.* **29** (2000) 49.
9. K. SATYAPRASAD, Y. R. MAHAJAN and V. V. BHANUPRASAD, *Scripta Metall.* **26** (1992) 711.
10. D. M. KOCHERGINSKY and R. G. REDDY, in Proceedings of *in situ* Reactions for Synthesis of Composites, Ceramics, and Inter-metallics—TMS Annual Conference, Las Vegas, Nev., USA, 1995, edited by E. V. Barrera, F. D. S. Marquis, W. E. Frazier, S. G. Fishman, N. N. Thadhani and Z. A. Munir (TMS, Warrendale, PA, USA, 1995) p. 159.
11. B. YUCEL, *J. Mater. Sci.* **34** (1999) 1653.
12. H. SCHOLZ and P. GREIL, *ibid.* **26** (1991) 669.
13. A. S. NAGELBERG, S. ANTOLIN and A. W. URQUHART, *J. Amer. Ceram. Soc.* **75** (1992) 455.
14. B. S. S. DANIEL and V. S. R. MURTHY, *Mater. Des.* **16** (1995) 155.
15. M. J. KOCZAK and K. SHARVAN KUMAR, US Patent 4,808,372 (1989).
16. M. G. CHU and M. K. PREMKUMAR, *Metall. Mater. Trans.* A **24A** (1993) 2803.
17. R. G. REDDY and BANQIU WU, US Patent 6,343,640 (2002).
18. B. WU and R. G. REDDY, *Metall. Mater. Trans.* B **33B** (2002) 543.
19. Q. HOU, R. MUTHARASAN and M. KOCZAK, *Mater. Sci. Eng.* A **195A** (1995) 121.
20. Q. ZHENG, B. WU and R. G. REDDY, *Adv. Mater. Eng.* **5** (2003) 167.
21. Q. ZHENG, R. G. REDDY and B. WU, in Proceedings of State of the Art in Cast Metal Composites in the Next Millennium—2000 TMS Fall Meeting, St. Louis, Missouri, USA, 2000, edited by P. K. Rohatgi (TMS, Warrendale, PA, USA, 2000) p. 1.
22. Q. ZHENG, B. WU and R. G. REDDY, in Proceedings of Affordable Metal-Matrix Composites for High Performance Applications—2001 TMS Fall Meeting, Indianapolis, Indiana, USA, 2001, edited by A. B. Pandey, K. L. Kendig and T. J. Watson (TMS, Warrendale, PA, USA, 2001) p. 199.
23. Q. ZHENG and R. G. REDDY, 2002 NSF Design, Service, and Manufacturing Grantees and Research Conference, Ames, Iowa, USA, edited by San Juan and Puerto Rico (Iowa State University, Ames, Iowa, USA, 2002) p. 2144.
24. *Idem.*, in Proceedings of 2003 NSF Design, Service and Manufacturing Grantees and Research Conference, Birmingham, Alabama, USA, 2003, edited by R. G. Reddy (The University of Alabama, Tuscaloosa, AL, USA, 2003) p. 30.
25. S. SWAMINATHAN, B. S. RAO and V. JAYARAM, *Mater. Sci. Eng.* A **A337** (2002) 134.
26. S. KRUKOWSKI, Z. ROMANOWSKI, I. GRZEGORY and S. POROWSKI, *J. Crys. Grow.* **189/190** (1998) 159.
27. G. F. FROMENT and K. B. BISCHOFF, in "Chemical Reactor Analysis and Design" (John Wiley & Sons, 1976).
28. M. BYRNE and G. R. BELTON, *Metall. Trans.* B **14B** (1983) 441.
29. S. POROWSKI, *MRS Inter. J. Nitride Semi. Re.* **4S1** (1999) G10.2.
30. D. L. SMITH, in "Thin-film Deposition: Principles and Practice" (McGraw-Hill, 1995) p. 120.

Received 28 February
and accepted 19 August 2003